Rover Publications
United International Journal of Engineering and Sciences (UIJES)
An International Peer-Reviewed(Refereed)Engineering and Science Journal;Impact Factor: 5.735(SJIF)
Vol-3,Issue-4 ,2022 ISSN:2582-5887 www.uijes.com

Control system hardware design and experimental analysis

Moukouyou Milebe Raphael,College of Automation,Major* Electrical Engineering,Nanjing University of Aeronautics and Astronautics, Nanjing 210016, China
Zhenyang Hao,Department of Electrical Engineering,Nanjing University of Aeronautics and Astronautics,Nanjing, China Center for More-Electric-Aircraft Power System, Nanjing University of Aeronautics and Astronautics, Nanjing, China
Dong Jiabao,,Department of Electrical Engineering,Nanjing University of Aeronautics and Astronautics, Nanjing, China

Article Received: 02/06/2022, Article Accepted:07 /10/2022, Published online: 10/10/2022,DOI:10.53414/UIJES.2022.4.02

Abstract
Position sensors, which monitor the voltage or current generated at a specific spatial point while the motor rotor is rotating, are not necessary for the construction of brushless DC motors. By altering the motor's speed, phase lag may be reduced as it fluctuates with it. For a complex system like a multi-copter, reinforcement learning neural networks are recommended as an efficient PID controller gain auto-tuning method.

Keywords: Position sensors, DC, Speed, rotor

I.Introduction

The PMSM uses a high-speed sensorless drive to determine the rotor position. Position sensorless control is preferred because it not only reduces system cost but also increases reliability and robustness [1]. The classic forward Euler-based discrete-time model may be unstable due to its inaccuracy in the high-speeds region where carrier frequency to fundamental frequency is generally low [2].

Brushless DC motors can be built without position sensors, which are used to track the voltage or current produced at a particular spatial location while the motor rotor is rotating. On the stator winding, a fast-running motor will exert a continually fluctuating counter-electromotive force. Reinforcement learning neural networks are suggested as an effective PID controller gain auto-tuning technique for a complicated system like a multi-copter.

II. Mathematical Model Permanent Magnet Synchronous Motor

A PMSM is defined as a three-phase smooth-air-gap machine that is symmetrical and includes windings that are dispersed sinusoidally. Three key components make up the mathematical model of the PMSM under consideration. Induction of electromagnetic force is assumed to be sinusoidal; eddy currents and hysteresis losses are not considered. There are no dynamical dependencies in the air gap, and there is no rotor cage.

$$\begin{aligned} u_A &= R_S i_A + \frac{d}{dt}\psi_A \\ u_B &= R_S i_B + \frac{d}{dt}\psi_B \\ u_C &= R_S i_C + \frac{d}{dt}\psi_C \end{aligned} \qquad (1.1)$$

Rover Publications
United International Journal of Engineering and Sciences (UIJES)
An International Peer-Reviewed(Refereed)Engineering and Science Journal;Impact Factor: 5.735(SJIF)
Vol-3,Issue-4 ,2022 ISSN:2582-5887 www.uijes.com

Flux equation

$$\begin{aligned}\psi_A &= L_{AA}i_A + L_{AB}i_B + L_{AC}i_C + \psi_r \cos\theta \\ \psi_B &= L_{BA}i_A + L_{BB}i_B + L_{BC}i_C + \psi_r \cos\left(\theta - \frac{2\pi}{3}\right) \\ \psi_C &= L_{CA}i_A + L_{CB}i_B + L_{CC}i_C + \psi_r \cos\left(\theta + \frac{2\pi}{3}\right)\end{aligned} \quad (1.2)$$

Electrical equations

$$\begin{aligned}v_d &= R_s \cdot i_d + l_{sd} \cdot \frac{di_d}{dt} - L_{sq} \cdot \omega_r \cdot i_q \\ v_q &= R_s \cdot i_q + l_{sq} \cdot \frac{di_q}{dt} + L_{sd} \cdot \omega_r \cdot i_d + \psi_{md} \cdot \omega_r \\ C_{em} &= p \cdot \left((l_{sd} - L_{sq}) \cdot i_q \cdot i_d + \psi_{md} \cdot i_q\right)\end{aligned} \quad (1.3)$$

Where i_d,i_q the stator currents; v_d,v_q stator voltages; R_s stator resistance; l_sd,L_sq stator inductances; ψ_mdPermanent magnet flux; p number of machine pole pairs; ω_r=𝑑i/𝑑t θ_r = p 𝑑i/𝑑t θ_m electric angular speed (pulsation) of the rotor; θ_m mechanical position of the rotor; C_em electromagnetic torque;

Using MATLAB, the mathematical modeling of a permanent magnet synchronous motor has been finished. The key component of PMSM is its high efficacy supplied with the proportion of information power after allowing for information influence's negative effects. The PMSM has no rotor current or field current. It assumes that permanent magnets rather than direct current excitation cause the armature emf [3].

III.EXPERIMENTAL VERIFICATION

A. Experimental platform construction

In order to realize the experimental debugging and analysis[4], the physical hardware motor control system is built as shown in figure 1.

Fig.1 Control system hardware circuit board

A brushless DC motor is connected to the magnetic particle dynamometer to facilitate the addition or reduction of load to the motor in working condition. Its power supply is external power supply, need external 3.3V raw control chip power supply and motor bus voltage. The application of MATLAB / Simulink to build a model, and the underlying software IAR to interface, the algorithm model to generate the C code suitable for the underlying compilation environment.

B. Speed estimation and delay programming

There are three kinds of digital speed measuring methods: M method, T method and M/T methods [5]. The rotating speed can be obtained by calculating the number of pulses in the given time. Average angular velocity during the commutation interval can be calculated by measuring the time interval between the two commutation pulses.

Fig.1 Control system hardware circuit board

Rover Publications
United International Journal of Engineering and Sciences (UIJES)
An International Peer-Reviewed(Refereed)Engineering and Science Journal;Impact Factor: 5.735(SJIF)
Vol-3,Issue-4 ,2022 ISSN:2582-5887 www.uijes.com

A brushless DC motor is connected to the magnetic particle dynamometer to facilitate the addition or reduction of load to the motor in working condition. Its power supply is external power supply, need external 3.3V raw control chip power supply and motor bus voltage. The application of MATLAB / Simulink to build a model, and the underlying software IAR to interface, the algorithm model to generate the C code suitable for the underlying compilation environment.

C. Speed estimation and delay programming

There are three kinds of digital speed measuring methods: M method, T method and M/T methods [5]. The rotating speed can be obtained by calculating the number of pulses in the given time. Average angular velocity during the commutation interval can be calculated by measuring the time interval between the two commutation pulses.

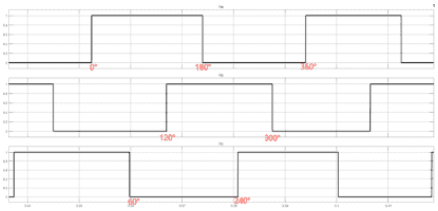

Fig.2 Three-phase commutation signal

The switching period is 20Khz, and the interrupt time of each EPWM is 50 us. The time interval is obtained by counting the number of PWM used to turn on the switch. For each interrupt, the count value tick1 is added to one, which is equivalent to an increase of 50 us of timing.

Due to the fact that the terminal voltage is at the same time as the $\frac{1}{2}u_{dc}$ when comparing, there may be a small jitter[6], resulting in many times to determine the trigger commutation signal, so it is necessary to limit the tickl count value, that is, filter the small tick1 count value; it has been calculated that at a speed of 500 rpm and frequency of 33 hz, the

$$\text{tick1} = \frac{T}{T_K} = \frac{1}{f \times T_K} = \frac{1}{33 \times 50 \times 10^6} \approx 606 \quad (1.4)$$

So, the high-level counts at 500 rpm are about 303;

Frequency of 316hz at a rated speed of 4750 rpm, the

$$\text{tick1} = \frac{T}{T_K} = \frac{1}{f \times T_K} = \frac{1}{316 \times 50 \times 10^6} \approx 63 \quad (1.5)$$

Then the count at the 1000 rpm high level is about 32;

At 500 rpm to 4750 rpm, the count value tick ranges from 303 to 32, so the count values less than 10 of tick1 are filtered; The number of interrupts is counted during the high level, the count value is alculated during the low level to obtain the rotational speed, The formula is:

$$n = \frac{60f}{4} = 15 \times T = \frac{15}{\text{tickl} \times 2 \times 50 \times 10^6} \quad (1.6)$$

among

$$\alpha = \frac{T}{T_f + T} = \frac{1}{f \times T_K} = 2\pi f T \quad (1.8)$$

The bulk of the utility model is composed of the isolation circuit, low pass filter circuit, and operational amplifier conditioning circuit [7]. The speed of the commutation signals of the three

phases is estimated. Calculate the frequency, period, and electrical angular velocity based on the anticipated rotating speed. Next, determine the end voltage detection of the hardware circuit in the filter delay caused by reference.

$$\alpha_1 = \arctan\left(\frac{\omega R_1 R_2 C_1}{R_1 + R_2}\right)$$
$$\alpha_3 = \arctan\left(\omega R_{15} C_{13}\right) \quad (1.9)$$

C.Experimental results

When I/F up to 500rpm, the estimated speed information is read by RS485 [5], the data waveform is shown in the figure below. Given the speed of 500rpm. the estimated rotational speed is about 460rpm with an error of 8%.

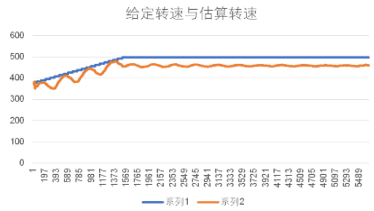

Fig.3. 500 rpm Given speed and estimated speed

At I / F up to 100 rpm, the estimated speed is about 980 rpm with an error of 2%. The data waveform is shown in Figure 4.

Fig. 4 Given and estimated rotational speed at 1000 rpm

In the experiment, it was found that there will be delay angle error, output commutation signal disorder, which shows that the program of delay output has errors. At present, it cannot solve the problem, but also needs to learn to write related programs [8]. If the speed fluctuations, the delay time will also have fluctuations, and the correct signal should be orange signal lag blue waveform about 1/4 cycle.

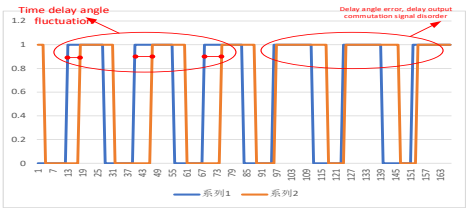

Fig. 5 Voltage sampling circuit

Rover Publications
United International Journal of Engineering and Sciences (UIJES)
An International Peer-Reviewed(Refereed)Engineering and Science Journal;Impact Factor: 5.735(SJIF)
Vol-3,Issue-4 ,2022 ISSN:2582-5887 www.uijes.com

D. Terminal Voltage Sampling Circuit

The terminal voltage sampling circuit parameters are calculated, the circuit is welded and debugged, and the terminal voltage sampling experiment is carried out [9]. The parameters of the terminal voltage sampling circuit are designed according to the bus voltage sample circuit of the actuator.

(1) Voltage divider filter circuit

The isolated chip ACPL-87B's input voltage range is 0 to 2volts, the bus voltage is 28volts, and the maximum duty cycle output is 0.9kohms. The first passive low pass filter circuit is made up of the resistors R1 and R2, which form a voltage circuit that weakens the strong signal of terminal voltage.

$$V_0 = V_{in} \times \frac{R_2}{R_1+R_2} = 28 \times 0.9 \times \frac{10K}{110K+10K} \approx 25.2 \times 0.083 \approx 2 \quad (1.10)$$

The maximum frequency at which the motor operates is:

$$f = \frac{p \times n}{60} = \frac{4 \times 4750}{60} \approx 316.67h \quad (1.11)$$

$$f_1 = \frac{R_1+R_2}{2\pi R_1 R_2 C_1} = 789hz \quad (1.12)$$

(2) Op amp conditioning circuit

The voltage signal of the voltage divider filter is isolated from the analog ground and the power ground by the isolation chip, and then a differential signal is output. The difference signal is sent to the operational amplifier circuit for conditioning. The operation amplifier simplified circuit is shown in Figure 5.

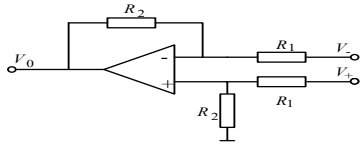

Fig. 5 Simplified operational amplifier circuit

Because the input impedance of the op-amp is approximately infinite, the "virtual short" and "virtual break" of the op amp is known:

$$\frac{V_- - V_+ \times \frac{R_2}{R_1+R_2}}{R_1} = \frac{V_+ \times \frac{R_2}{R_1+R_2} - V_0}{R_2} \quad (1.13)$$

$$V_0 = \frac{R_2}{R_1}(V_+ - V_-) \quad (1.14)$$

Since the voltage divider converts the terminal voltage into a voltage signal of up to 2V, the input voltage range of the DSP I/O port is 0-3V, so the choice, by substitution, gives:

$$V_0 = (V_+ - V_-) \quad (1.15)$$

(3) Low-pass filter circuit.

Before the terminal voltage signal is sent to DSP, it is filtered again. If R15 = 2KΩ, C13 is 0.1uF, the cutoff frequency is

$$f_1 = \frac{1}{2\pi R_{15} C_{13}} = 795hz \qquad (1.16)$$

E. Simulation Verification

When the I/F stage runs at 500rpm, the terminal voltage waveform after filtering according to the actual selected partial voltage filter parameter is shown in Figure 6. Most of the high-frequency interference signals can be filtered under this parameter. After cut-in back EMF zero-crossing detection, this situation is eliminated due to the small phase difference between the estimated angle and the actual angle, as shown in Figure 7.

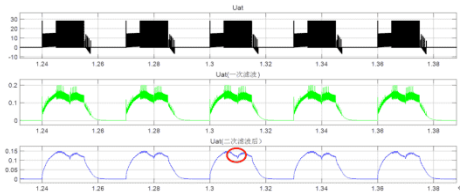

Fig. 6 I / F Stage Terminal Voltage

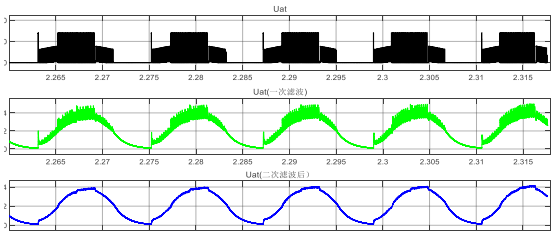

Fig.7 Terminal voltage of back EMF at zero-crossing stage

F. Experimental Testing

Figure 8 shows the line current and terminal voltage signals of the motor running at 500 rpm. The pink waveform is the differential signal which is isolated by the chip output after the voltage divider is filtered. Because the voltage is small, the scope of the oscilloscope is 250 mV, and the differential probe itself will have some clutter. The filter is sent to DSP after the operation amplifier on the board is adjusted.

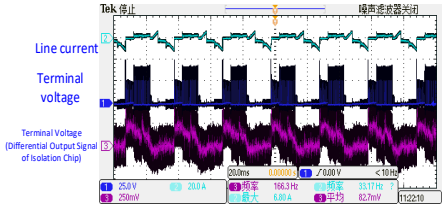

Fig. 8 Line current and terminal voltage

The three-phase terminal voltage waveform read by RS485 is shown in Figure 9, because of the simultaneous acquisition of three signals [10]. The actual signal is expanded 1000 times for data transmission, so the accuracy of data acquisition is not high. At the top of the end voltage, the lower

bridge arm has a concave trend, and at the bottom of the voltage difference of 120 °, basically can judge the acquisition of terminal voltage signal is correct.

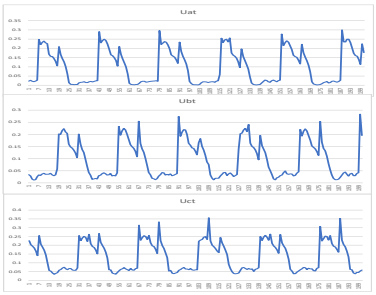

Fig. 9 RS485 reading terminal voltage data

To obtain the commutation signal waveform illustrated below, the phase A voltage is compared to 1 / 2Udc, however the real commutation signals must have a 90° lag depending on the frequency information.

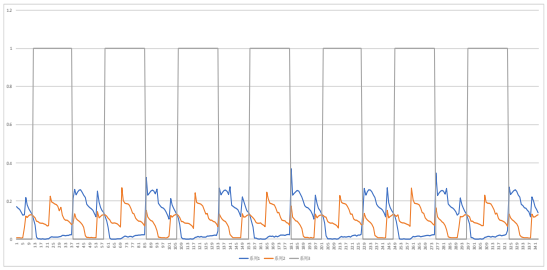

Fig.10 RS485 reading terminal voltage and commutation signal data

FIG. 11 shows the I / F given commutation signal read by RS485 and commutation signals obtained by terminal voltage judgment, selecting the same amount of data, the width of commutation signal is the same, so the correctness of terminal voltage acquisition can be judged.

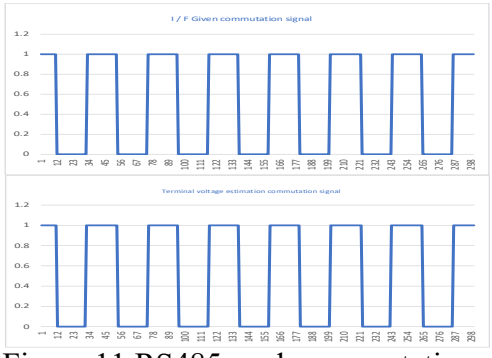

Figure 11 RS485 reads commutation signal data

IV. BOOSTING EXPERIMENT AND ANALYSIS OF CURRENT SPIKE PROBLEM

A. Speed-up experiment

When speeding up to 2500rpm, it was found that the end voltage and line current waveforms were asymmetrical, as shown in the left panel of figure 12. After compensating for the delay angle of about 7.2°, the line current and terminal voltage waveforms are basically symmetrical, and the current

amplitude drops slightly. As the speed rises, the commutation signal will gradually advance, and at 3000rpm, the compensation angle is about 14°.

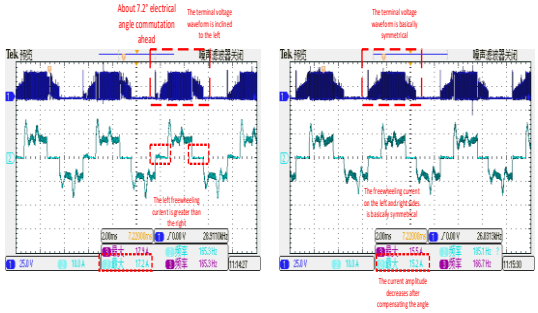

Fig.12 End voltage and line current (2500rpm)

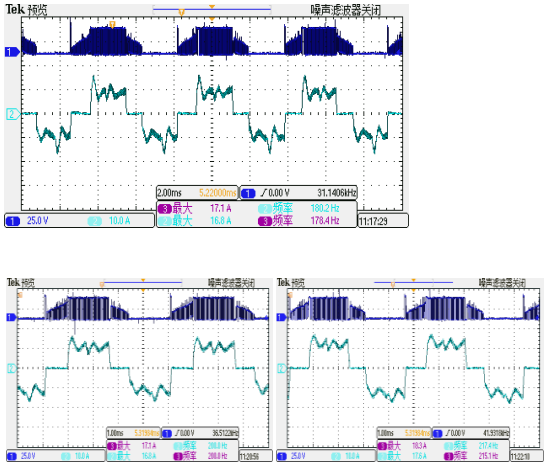

3000rpm 3200rpm

Fig. 13 Terminal voltage and line current

B. 2.Current spike problem

During the acceleration, it is found that whenever the upper bridge arm is commutated, a relatively large current spike will be generated, as shown in the figure below.

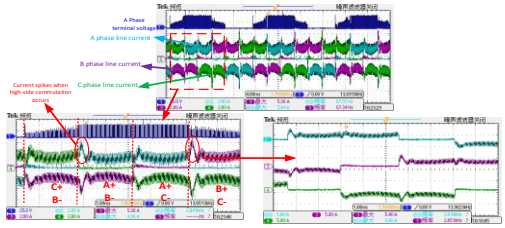

Fig.14 Three-phase line current

(1) RS485's low acquisition rate causes the influence of the feedback current to occur mostly when the 2-sector commutates to the 6-sector, or from B+ A- to C+ A-, or the time the top tube is commutated. When operating at 1000 rpm, it is discovered that the speed loop outputs a reference

current that is comparatively steady, indicating that the current spike is not caused by fluctuations in the provided current.

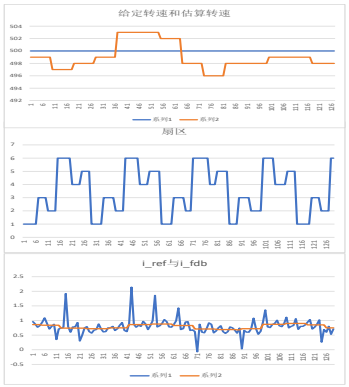

(2) Measure the output duty cycle at the time the upper tube is commutated. The red box in the figure below will switch from B+ A- to C+A-, giving a given current of 4A and a feedback current of approximately 5.8A. The experimental waveform shows that the feedback current is less than the reference current in the first cycle. This causes the second cycle to continue with output duty, even though theoretically the third cycle duty cycle should be zero.

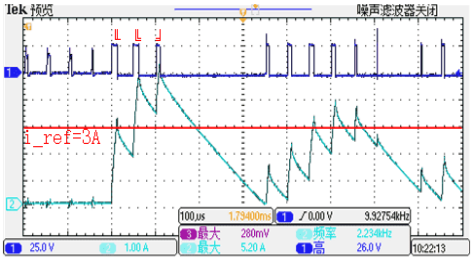

IV. CONCLUSION

The ACPL-87B's input voltage range is 0 to 2 volts, the bus voltage is 28volts, and the maximum duty cycle output is 0.9kohms. The bulk of the utility model is composed of the isolation circuit, low pass filter circuit, and operational amplifier conditioning circuit. Most of the high-frequency interference signals can be filtered under this parameter. Reinforcement learning neural networks are suggested as an effective PID controller gain auto-tuning technique for a complicated system like a multi-copter.

REFERENCE

[1] G. Wang, M. Valla and J. Solsona, "Position Sensorless Permanent Magnet Synchronous Machine Drives—A Review", IEEE Trans. Ind. Electron, vol. 67, no. 7, pp. 5830-5842, Jul. 2020.

[2] H. Kim, M. W. Degner, J. M. Guerrero, F. Briz and R. D. Lorenz, "Discrete-Time Current Regulator Design for AC Machine Drives", IEEE Trans. Ind. Appl, vol. 46, no. 4, pp. 1425-1435, Jul. 2010.

[3] Bhatti P, Hannaford B (1997) Single-chip velocity measurement system for incremental optical encoders. IEEE Trans Control Syst Technol 5(6):654–661

[4] Zhang Fang'e, Heng Junshan, and Zhen Huanqiang, Research on reliability of RS485 bus network. Chinese Journal of Scientific Instrument, Vol.27 No.6, PP.2458-2459, Jun 2006(In Chinese).

[5] P. Pillay and R. Krishnan, "Modeling, Simulation, and Analysis of Permanent Magnets Motor Drives, Part I: The Permanent Magnet Synchronous Motor Drive", IEEE Trans. on Industry Applications, Vol. 25, No. 2, March/April 1989, pp. 265-273.

[6] A. Consoli, G. Scarcella and A. Testa, "Industry application of zero-speed sensorless control techniques for PM synchronous motors," in IEEE Transactions on Industry Applications, vol. 37, no. 2, pp. 513-521, March-April 2001, doi: 10.1109/28.913716

[7] K. Koga, R. Ueda, T. Sonoda, "Constitution of V/f control for reducingsteady state error to zero in induction machine drive to zero in induction machine drive system"; IEEE Transactions, vol. IA-28, no.2, 1992, pp.463-471;

[8] V. I. Utkin, "Sliding mode control design principles and applications to electric drives," in IEEE Transactions on Industrial Electronics, vol. 40, no. 1, pp. 23-36, Feb. 1993, doi: 10.1109/41. 184818..

[9] Z. Wang, K. Lu and F. Blaabjerg, "A Simple Startup Strategy Based on Current Regulation for Back-EMF-Based Sensorless Control of PMSM," in IEEE Transactions on Power Electronics, vol. 27, no. 8, pp. 3817-3825, Aug. 2012, doi: 10.1109/TPEL.2012.2186464.

[10] J. Xing, Z. Qin, C. Lin and X. Jiang, "Research on Startup Process for Sensorless Control of PMSMs Based on I-F Method Combined with an Adaptive Compensator," in IEEE Access, vol. 8, pp. 70812-70821, 2020, doi: 10.1109/ACCESS.2020.2987343

How to cite this article?

***Moukouyou Milebe Raphael** ," Control system hardware design and experimental analysis ",United International Journal of Engineering and Sciences (UIJES) 3 (4), PP: 38-47,2022, DOI:10.53414/UIJES.2022.4.04